

Characterization and Modeling of the Capacitive HBC Channel

M. D. Pereira, *Member, IEEE*, G. A. Alvarez-Botero, *Member, IEEE*, and F. R. de Sousa, *Member, IEEE*

Abstract — Increasing interest in wireless body area networks has created the need for alternative communication schemes. One example of such schemes is the use of the human body as a communication medium. This technology is called human body communication (HBC) and it offers advantages over the most common radiation-based methods, which makes it an interesting alternative to implement body area networks. The aim of this study was to identify the influence of a fixture on the HBC channel characterization and an extended model, which includes the test fixtures, to explain the measured channel response is proposed herein. The model was tested against channel measurement results and good experiment-model correlation was obtained. The results show that the test fixture has a non-negligible influence, and that an extended model, based on the physical meaning of the phenomena involved, helps to explain the channel frequency profile results and behavior.

Keywords — WBAN, HBC; IBC; BCC; capacitive coupling; fixture influence, channel modeling.

I. INTRODUCTION

Human body communication (HBC) technology, also known as body coupled communication (BCC) or intra-body communication (IBC), was first proposed by Zimmerman in 1995 [1], when he realized he could modulate the electric field used for position measurements to transmit data. HBC has recently emerged as an alternative that could overcome most of the challenges associated with wireless body area networks (WBANs), which are related to the pursuit of devices with low power, communication reliability, high data transmission rates and a high level of data security and privacy [2],[3].

In HBC the human body is used as the main transmission medium for the communication of signals between a transmitter and a receiver. The signal of the transmitter is electrically coupled to the body through electrodes instead of an antenna, and is captured at another part of the body by a receiver using similar electrodes. The operating frequency is usually higher than 0.1 MHz, to avoid electromagnetic interference, and lower than 100 MHz, to minimize the radiation of the signal out of the body. These characteristics give the following advantages to HBC when compared to the wireless methods available: it is

less sensitive to electromagnetic interference, provides higher data communication security and presents higher spectral efficiency [1], [4], [5]. Operation at low frequency also allows the potential to eliminate power-hungry RF front-end circuits, since the signals can be processed by baseband digital and analog low-power circuits.

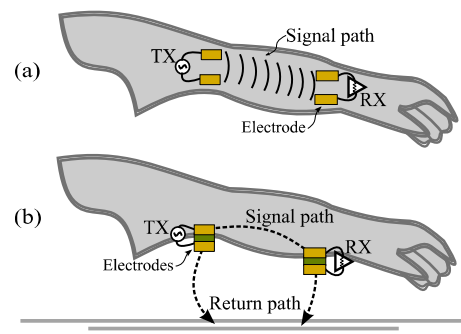


Fig. 1. HBC coupling methods: (a) galvanic and (b) capacitive.

HBC signals are coupled to the body using two methods: capacitive coupling and galvanic coupling [6]. In the galvanic coupling technique (Fig. 1-a) a pair of electrodes is in contact with the skin at the transmitter (Tx) and couples the signal to the body generating a differential signal which induces galvanic currents. The signals are captured by another pair of electrodes in contact with the skin at the receiver (Rx) [7], [8]. The absence of external ground makes this method independent of the environment and suitable for wearable and implantable devices. However, it has been shown that it only works acceptably with short distances (~15 cm) between the transmitter and the receiver and at frequencies below 1 MHz, limiting data transmission rate [7], [10].

In capacitive coupling (Fig. 1-b) one of the transmitter electrodes is attached to the skin and the other is kept floating. In this way, the transmitter generates an electric potential, inducing an electric field in the body that is sensed by the receiver electrodes arranged in the same way. The floating electrodes are coupled to ground through the air, creating a return path, while the signal electrodes in contact with the skin create the forward path of the signal [11]. The existence of an external path means that capacitive coupling is only suitable for wearable devices and is sensitive to environmental interference. Nonetheless, it has higher gain [5] and a relatively higher frequency range of operation, between 1-100 MHz, which enables higher data transmission rates than the galvanic coupling

M. D. Pereira, G. A. Alvarez-Botero and F. R. de Sousa are with the Radio Frequency Research Group, Federal University of Santa Catarina (UFSC) Florianópolis-SC, Brazil (e-mail: {maicondeivid, g.a.alvarez, rangel}@ieee.org).

method [10], [12], [13]. In the remainder of this paper only the capacitive coupling method is of concern.

Characterization of the HBC channel is essential for developing models which can aid the design of transceivers to meet the low power requirements of WBANs. The output power and the input sensitivity of a transceiver are both related to the channel frequency response and they play an important role in the determination of the system power consumption.

Since the proposal of HBC, characterization and modeling have been a subject of discussion, mostly due to the dependence of the results on the measurement methodology and the challenges associated with preserving the correct channel path within the body [4], [11], [14], [15]. In this regard, Callejón *et al.* [10] proposed a body channel transmission model based on skin impedance and admittance derived from the skin cell dimensions and electrical characteristics. However, this is not a complete channel model, since it does not directly model the return path or leakage capacitances, the values used being taken from the literature. Also, during the validation through measurements taken using a spectrum analyzer with baluns, only the insertion loss of the baluns and cables were considered in the measurements. In [16], Bae *et al.* presented a channel model based on the theoretical solution of the electrical field from an infinitesimal dipole on the surface of the body, describing the path loss according to distance and frequency. However, the channel dependence on the return path was not explicitly included in the analysis. Additionally, in the measurements with a battery-powered signal generator as the transmitter and a balun-isolated spectrum analyzer as the receiver, no attempt at fixture compensation was presented. In [13], Xu *et al.* created a circuit model from 3D electromagnetic (EM) simulation results obtained for different body members. It explicitly models the forward and return path, including some leakage and indirect signal paths. However, in the measurement setup, despite the ground isolation for the battery-powered transmitter, the receiver was connected to the earth ground through the power line, effectively increasing the channel gain. In addition, no fixture compensation was attempted and, therefore, no experimental verification was performed for a realistic HBC channel, with both ground electrodes of the transmitter and receiver floating. Overall, these references either lack a complete channel model or they do not make a substantial assessment of the test fixture influences, mostly performing only simple path loss corrections. Thus, this leads to different model outcomes which are not able to fully describe the channel measurement results.

This paper proposes a model that extends those currently available in the literature and aims at improving channel predictions for tests performed with laboratory equipment and accessories. The HBC channel, referred to herein as the primary channel, is presented with a clear division between its intrinsic and extrinsic parts that helps the channel identification and modeling procedure. A measurement setup is analyzed and the influence of its components is accounted for in an extended model, based on a mixed distributed-lumped representation of the primary channel parts and a test fixture setup. The new channel model is supported by the physical behavior of each component. Finally, the extended model is analyzed and compared to the primary channel model and channel characteriza-

tion results to assess its capability to explain and represent channel measurements, showing the need to properly account for the test fixture when characterizing the channel and pointing out to the expected attenuation levels of the real HBC channel profile.

In order to gain a better understanding of HBC systems, the following sections identify the primary HBC channel, describe some useful models available in the literature, analyze and model the test fixture influences, discuss the complete HBC setup modeling, and compare the channel characterization results for the proposed model.

II. PRIMARY CHANNEL MODELING

One of the most important aspects associated with properly characterizing and modeling the HBC channel is the identification of the correct primary channel. Failure to recognize this could lead to a channel response that resembles low-pass profiles or higher channel gain [17], [18]. The other important aspect is to consider the influence of the measurement setup on the results. Let us address the channel identification issue first. The division of the HBC path into its essential parts facilitates this task. In this paper, the primary capacitive HBC channel is divided into an intrinsic and an extrinsic part. The intrinsic part is the direct path through the body between the signal electrodes, as shown in Fig. 2, which should be modeled basically by the electrical properties of the tissues. This intrinsic section can be considered static, since it does not change with the external conditions, being only dependent on the distance of propagation over the body. The extrinsic part is the return path through the air between the external ground plane and the ground electrodes, including alternative signal paths that would probably be seen in the real channel as signal leakage directly from the body to the electrodes or the ground plane. The interfaces between the transceivers and the body, *i.e.*, the electrode pairs, are also parts of the extrinsic channel, as shown in Fig. 2. The extrinsic portion of the channel is dependent mostly on the environment, the distance from the ground, the presence of objects in the return path, the electrodes and their contact with the skin.

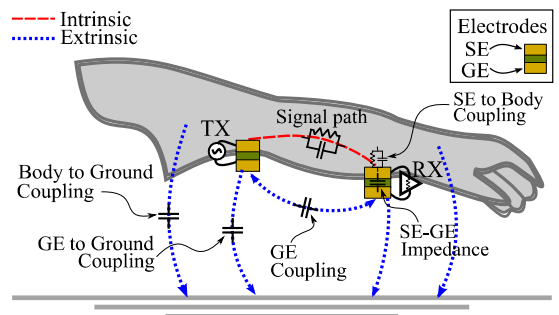


Fig. 2. Capacitive coupling HBC primary channel with its intrinsic and extrinsic parts (GE = Ground Electrode, SE = Signal Electrode).

Equivalent circuit models are preferred to describe the HBC channel, since they present a more intuitive and practical visualization of the channel response than theoretical electromagnetic or 3D-simulation models. In Fig. 3, a circuit diagram shows the essential components to be modeled to reproduce the

primary channel behavior. The intrinsic channel is represented by C_{body} and R_{body} , which here only exemplify a lumped or distributed model for the body tissues. The extrinsic channel part is comprised of C_e (which models the inter-electrode capacitance), $C_{es}R_{es}$ (which models the electrode-skin RC impedance), C_{ret} (which models the transceiver ground electrode coupling to the external ground), C_x (which models the direct cross-coupling between ground electrodes from the transmitter and receiver), and C_{leak} (which is the leakage capacitance that represents each unit length body segment coupling to the external ground). In the following sections, the determination of these circuit models for the intrinsic and extrinsic parts of the body channel will be discussed.

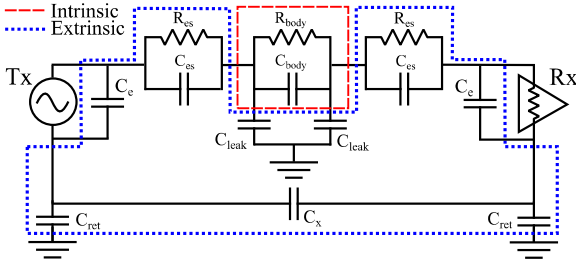


Fig. 3. Capacitive HBC primary channel circuit model.

A. Model for Intrinsic Part

Traditional electrical models of tissues aim to capture the cell membrane capacitive behavior and the extra- and intracellular liquid conductive aspect over frequency [19], as shown in Fig. 4, where the current paths around and inside the cells of the tissues are depicted. The simplest model capable of representing the electrical characteristics of the tissues over frequency uses only two components forming a single parallel RC circuit [10], [20], whose values are dependent on the cross-sectional area A , length L and dielectric properties (through $R = L/\sigma(\omega)A$ and $C = \epsilon_r(\omega)\epsilon_0A/L$) of each tissue. In these expressions, the dependence of the relative permittivity $\epsilon_r(\omega)$ and conductivity $\sigma(\omega)$ of the tissues on the frequency must be properly modeled using the Cole-Cole or Debye models [21], [22], [23]. Since these parallel RC circuits model individual tissues over length and area, they must be properly connected to create a network that can represent the longitudinal and transversal signal propagation path over the body tissues. This tends to create complex circuit networks when the many tissue layers in the body are considered [20].

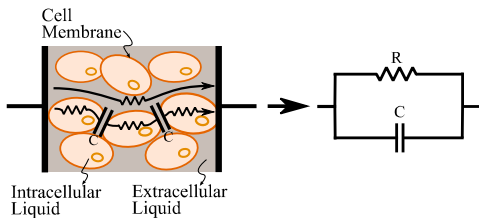


Fig. 4. Model of human body tissue which captures the electrical behavior of its cells and fluids.

To avoid this cumbersome representation, the segmentation of the body into unit length blocks combined with 3D EM

simulation can be used and single lumped RC blocks can then be extracted for each segment [13], [18]. In the distributed-network body model described in [13] the intrinsic part of the channel is modeled by the cascading of unit length RC circuit blocks for the arms and torso, as shown in Fig. 5 (a) and (b), respectively. The components $C_{(arm, chest, torso)}$ and $R_{(arm, chest, torso)}$ form the equivalent model for the composite effect of the body tissues in each segment. The unit blocks also include C_{leak} , since leakage occurs from each body segment to ground, as discussed in Section II.B.I.1 The authors of [13] estimated the component values of the model from 3D EM simulations of segments measuring 10 cm in length for the arms and 40 cm for the torso (including the chest) of a body. This model will be adopted as the reference for the intrinsic part of the primary channel model proposed in this article, replacing R_{body} and C_{body} in Fig. 3. The values for the components in each unit block are given in TABLE I. Compared to the models in [10], [16] and [18], this representation provides a better prediction of the intrinsic path since it considers the combined effect of multiple tissues in the body. Also, the explicit circuit representation is more suitable for accommodating changes to the basic core or additions to include parasitic effects and the fixture influences than other models such as the transmission line model in [10]. Additionally, the model is able to represent general body measurements, since the tissue parameters do not need to be changed to account for the use of different subjects, as this usually has a negligible effect on the channel response [24].

It should be noted that these circuit models are valid within a limited frequency range, since they cannot reproduce the high frequency signal behavior, when the wavelength approaches the human body dimensions, and the body starts to radiate the signals [18].

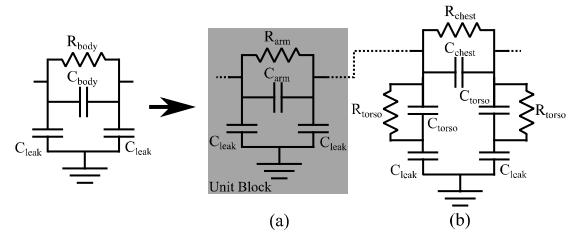


Fig. 5. Distributed-network circuit model representing a 10 cm unit block for the arm (a) and 40 cm unit block for the torso (b) [13].

TABLE I. DISTRIBUTED NETWORK ARM, CHEST AND TORSO COMPONENT VALUES [13].

R_{arm}	65 Ω	C_{chest}	3.5 pF
C_{arm}	25 pF	R_{torso}	600 Ω
R_{chest}	500 Ω	C_{torso}	4 pF

B. Model of Extrinsic Part

The model for the extrinsic part of the channel should include the return path capacitances, the models related to the electrodes, and leakage from the body parts to the electrodes

or the ground plane. These parts must be modeled considering the conditions of the tests performed on the primary channel.

1. Return Path Capacitances

There are basically three capacitances to be modeled regarding the return path: C_{ret} for the ground electrode to ground plane, C_x for the direct cross-coupling between ground electrodes and C_{leak} for the body to ground plane coupling.

The capacitance C_{ret} was estimated using an empirical expression for the capacitance of plates separated by long distances [26], [27] for two square copper electrodes of side lengths $L = 2$ cm and $L = 5$ cm, and with a variable distance h from the ground. The results were compared with C_{ret} extracted individually through a 1-port 3D EM finite element method (FEM) simulation over a semi-infinite ground plane, as shown in Fig. 6. A comparison between the capacitances extracted from the application of the empirical approximation and the performed simulations is shown in Fig. 7, for the two electrode side lengths over the distance h . The results show that larger ground electrodes give higher C_{ret} values. Regarding the error between the estimation methods, for a 5 cm side length electrode the largest discrepancy is of 20.4 % in the estimated capacitance, while for an electrode of 2 cm side length it is of 15.5 %, and decreases for long distances from the ground, asymptotically converging to a minimum limit value. Despite the potential of larger electrodes to increase the channel coupling, given the lower impedance present in the return path, the 2 cm side length is suitable for practical wearable applications and is adopted in this work. With this electrode size, for distances from the ground plane $h > 50$ cm, C_{ret} is around 870 fF.

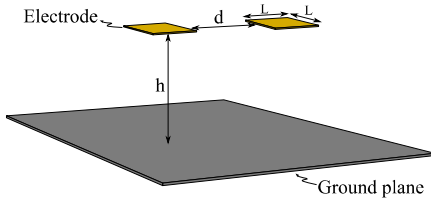


Fig. 6. Simulation setup for the extraction of the cross capacitance between electrodes, C_{cross} , and the ground coupling capacitance, C_{ret} .

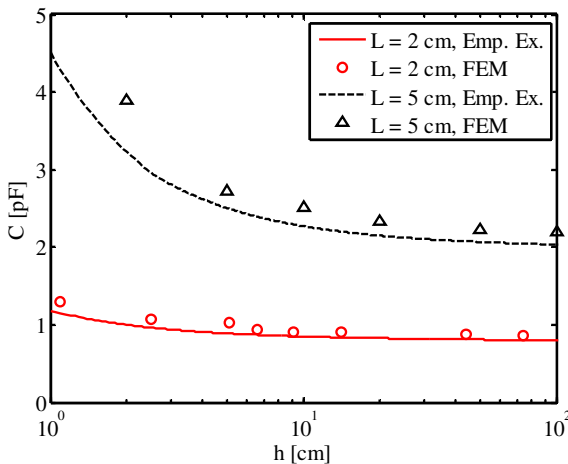


Fig. 7. Ground coupling capacitance, C_{ret} , according to distance h from the ground plane for empirical expression (Emp. Ex.) and 3D EM simulation (FEM).

In general, only the coupling from the ground electrode to the ground plane is modeled, since this is the dominant path, but for short distances between the transmitter and the receiver there is direct coupling through air, between the ground electrodes from the transmitter and the receiver, which must be considered [13]. This cross capacitance, C_x , which occurs between the ground electrodes of the transmitter and the receiver was extracted from 2-port 3D EM simulations of 4 cm^2 electrodes, with a horizontal distance between the plates of $150 \text{ cm} > d > 5 \text{ cm}$ and height from the ground plane of $h = 75 \text{ cm}$. The value obtained for C_x is presented in Fig. 8. The value for C_x is lower than $C_{ret}/10$ for distances greater than 5 cm between the Tx-Rx electrodes, and C_x still has a non-negligible effect on the channel response, as will be shown below.

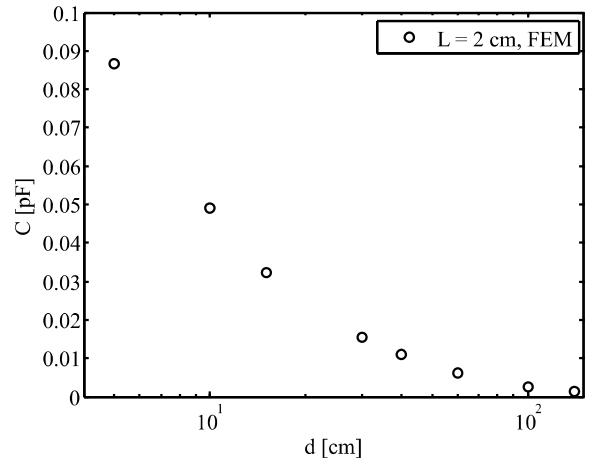


Fig. 8. Cross capacitance, C_x , according to the separation between Tx - Rx electrodes.

The leakage capacitance that appears from the body to external ground has been modeled in the literature assuming a distributed effect. Using a unity length division of the body parts, this capacitance was roughly estimated in [18] assuming that each segment is a conductive sphere over the ground with a diameter equal to the segment length. In [13] these capacitances were extracted through 3D EM simulations for the arms and torso. This is a more reliable method since it is performed in realistic body segments, instead of conductive spheres, and takes into account the multiple tissue layers and dielectric properties of the body. The simulation conditions in [13] are similar to the measurement conditions of this work and thus the values obtained for the leakage capacitances were adopted in the model presented in this article. The values of C_{leak} for the torso and arms were 0.7 pF and 15 pF, respectively, for each unit block, as shown in Fig. 5.

The coupling from the body parts to the ground electrodes has an insignificant effect on the channel response [18] and its influence can be neglected in the present analysis.

2. Electrode Impedances

In the capacitive HBC, one pair of electrodes is used by each transmitter and receiver. The electrode pair is comprised of a signal electrode, in contact with the skin, and a ground electrode, kept floating to form the return path over the air, as shown in Fig. 9. Three impedances related to these electrodes can be identified: a signal-ground pair impedance, each individual electrode impedance, and an electrode-skin impedance.

The pair impedance is dependent on the arrangement of the electrodes. The electrode pair shown has a vertical structure, with signal and ground electrodes separated by a dielectric. This creates a capacitance between the electrodes that can be modeled as a common parallel plate capacitor, with $C_e = \epsilon L^2/d$, where, ϵ is the permittivity of the material between the electrodes, L is the length of the electrodes and d is the distance between them. For 4 cm² copper electrodes, separated by a 0.15 cm thick FR4 dielectric, the capacitance is $C_e = 11.3$ pF. For the electrode itself the representation is dependent on the material and type of electrodes [28]. In this work, a bare copper electrode is used and it is approximated as a perfect conductor.

For a signal electrode in contact with the skin, the model is dependent on the type of electrode contact [28]. However, the channel gain does not change considerably for different electrode types as shown in [11], [24], [25]. Thus, a basic electrode-skin model could be developed from the following principles: the electrode can be viewed as one plate of a parallel plate capacitor due to its conductive characteristic. The other plate is formed by the more conductive tissue below the epidermis, which effectively works as a dielectric, as shown in Fig. 9 [28], [29]. This structure forms a capacitance with losses at the skin-electrode interface. Measurements of this interface impedance show that, for copper electrodes, it decreases with frequency in the range of interest [11], [25], showing the expected capacitive behavior. Therefore, the basic equivalent circuit of the contact impedance would include a capacitance C_{es} and a parallel resistance R_{es} , which models the epidermis conductance. The intrinsic channel in [13], accounts for the electrode-skin impedance effect within the model structure by means of slightly modified unit blocks for the region where the signal electrodes are in contact with the skin. This modified unit length block has the same structure as the arm block presented in Fig. 5(a), but with C_{arm} and R_{arm} replaced by $C_{injection} = 5.5$ pF and $R_{injection} = 250 \Omega$ [13], to account for the contact impedance.

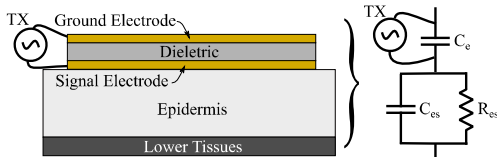


Fig. 9. Signal-ground electrode pair impedance and electrode-skin contact impedance models for copper electrodes.

C. Primary Channel Simulation

A 2-port S-parameters simulation based on the primary channel model shown in Fig. 3, with the value for the model elements defined in the previous sections, was performed for

different distances between the Rx and Tx electrodes, and for a total body length of 70 cm for each arm and 40 cm for the torso. The results are shown in Fig. 10. Note in this figure that the channel model shows a high-pass profile due to the ground coupling capacitance in the return path. At low frequency, the direct coupling capacitance between ground electrodes gives a distinct gain to each distance of propagation over the body. As the frequency increases, the tissue impedance becomes important and the gain has a higher dependence on the distance of the propagation. Thus far, this is the expected channel response if the test fixtures are neglected. The model has to be extended to represent the channel measurement results obtained on conventional laboratory equipment, because of the significant influence of the experimental setup on the HBC channel. This is addressed in the next section.

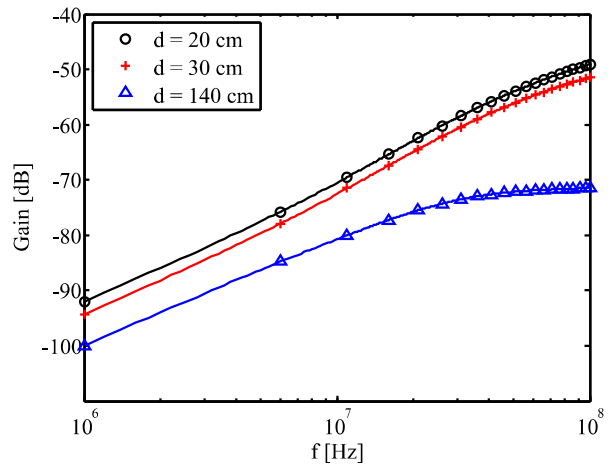


Fig. 10. Primary channel model gain simulation for three propagation distances over the body: $d = 20$ cm, 30 cm and 140 cm.

III. EXTENDED MODEL

The models presented in [10], [13], [16], [18] present some inaccuracies on reproducing real HBC channel results. The causes could be modeling simplifications or limitations, given the dynamic nature of the channel, especially as the frequency increases and the wavelength approaches the dimensions of the human body, allowing more signal leakage by radiation [16]. However, the divergences could also be related to fixture influences. In the distributed circuit models of both [13] and [18] the circuit simulation results were only compared to measurements taken from setups that did not fully address the issue of grounded equipment at the receiver, which effectively shunts part of the extrinsic channel and boosts the signal gain. The models of [10] and [16] were tested against measurements obtained from setups composed of a spectrum analyzer with baluns for ground decoupling. However, despite taking care to maintain the extrinsic path, the fixture non-idealities were not considered and, as will be shown next, this could be crucial in relation to properly explaining the measurement results. The next sections describe the measurement setup used for the channel characterization in this work and the extended channel model.

A. Measurement Setup

An illustration of the measurement system can be seen in Fig. 11. The fixture A and fixture B sections define the parts that are considered external to the body channel, while the DUT (device under test) section defines the extrinsic and intrinsic parts of the primary HBC. The test setup revolves around a two-port Rohde & Schwarz ZVB Vector Network Analyzer (300 KHz - 8 GHz). Baluns were necessary to decouple the HBC ground from that of the VNA ports which are internally connected and otherwise would bypass the floating return path in the extrinsic channel. The balun models used were the FTB-1-6 and FTB-1-1, from Mini-circuits, with effective frequency ranges of up to 125 and 500 MHz, respectively. The signal is fed to the body through adapted electrodes using coaxial cables. In this setup, a potential source of influences, excluding the ground of the VNA ports previously addressed with the baluns, is the transitions between the cables and electrodes, and the balun transformer itself. These will be discussed in the next sections.

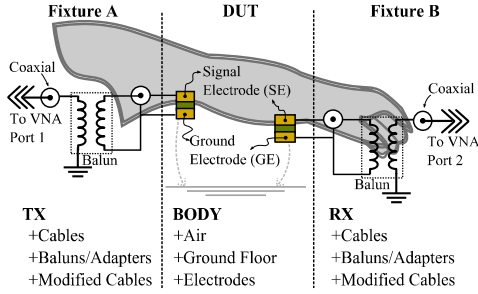


Fig. 11. Illustration of the measurement setup used to characterize the HBC channel splitting fixtures and device under test (DUT).

1. Cables and transitions

The cable attenuation and phase deviation can be measured and accounted for using transmission line models when necessary. Additionally, the transition of the coaxial cable to the electrodes must be modeled to account for its influence on the results. This transition is similar to the coaxial-to-PCB transitions and its basic model, presented in Fig. 12-a, has an $L_t C_t$ circuit with values usually extracted experimentally [30]. Since the cables were welded to electrodes without connectors, this experimental model extraction was not possible. However, the transition inductance was approximated by the inductance of a wire with 1 cm length and 0.1 cm diameter, as $L_t = 6$ nH. The capacitance C_t appears in parallel with the balun distributed capacitance and will be merged with it.

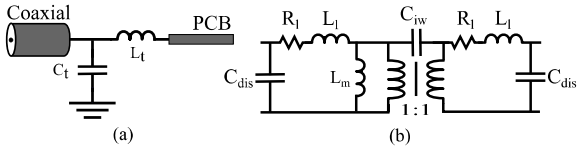


Fig. 12. Coaxial to microstrip transition LC (a) model and Balun transformer model (b).

2. Baluns

Until recently the influence of the balun on the HBC channel response had not been properly addressed and only its insertion loss was taken into account and removed via calibration. However, the balun interwinding capacitance, C_{iw} , has a non-negligible value and creates a path between the primary and secondary windings of the balun [31]. This jeopardizes the isolating property of the balun, creating an additional signal path between the transmitter and the receiver, directly through the VNA internal ground which boosts the channel gain. Another unwanted effect of the baluns is the distributed winding capacitance, C_{dis} , on the primary and secondary windings, shown in Fig. 12-b. The inductances related to the leakage and magnetizing flux, L_l and L_m , respectively, as well as the leakage inductance series resistance, R_l , can interfere with the channel frequency profile and are also present in the balun transformer model in Fig. 12-b [32], [33].

These components are not easy to estimate analytically and will be extracted experimentally [34] to be included in the model. The inductance L_l and its series resistance can be estimated with an impedance measurement of the primary winding, while the secondary winding is shorted, as shown in Fig. 13 (a). An open circuit impedance measurement, given in Fig. 13 (b), provides L_m . This measurement is also used to obtain the value for C_{dis} , since at high frequency the open impedance resonates and becomes capacitive. The capacitance C_{iw} is extracted by measuring the impedance between the primary and secondary windings when both are shorted, as shown in Fig. 13 (c). The measurements were taken on an Agilent 4294A LCR meter with the Fixture 16047E properly calibrated. The results for the two types of baluns analyzed here are summarized in TABLE II.

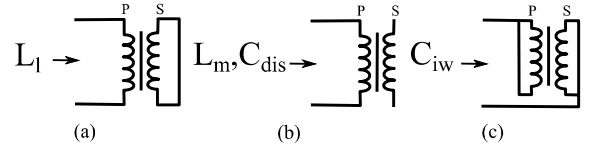


Fig. 13. Setups for measurement of the balun model parameters: (a) short-circuit, (b) open-circuit and (c) short-short configurations. P is the primary winding and S is the secondary winding.

TABLE II. MEASURED INTERWINDING AND DISTRIBUTED CAPACITANCES.

Component	Balun A	Balun B
Interwinding Capacitance (C_{iw})	27.2 \pm 0.2 pF	8.6 \pm 0.1 pF
Distributed Capacitance (C_{dis})	12.3 \pm 0.1 pF	9.3 \pm 0.1 pF
Leakage Inductance (L_l)	420.0 \pm 3.4 nH	246.0 \pm 2.0 nH
Leakage Resistance (R_{Ll})	13.0 \pm 0.1 Ω	4.0 \pm 0.1 Ω
Magnetizing Inductance (L_m)	200.0 \pm 1.6 μ H	30.6 \pm 0.2 μ H

B. Extended model analysis

Once the body channel and test fixture effects are determined, their combined influence is included in an extended channel model, shown in Fig. 14. The channel response over frequency and distance for the extended model appears in Fig.

15, for Balun A, with cables of around 70 cm and 4 cm² copper ground and signal electrodes. For illustrative reasons, the response of the primary channel, presented in Fig. 10, is included again in this figure.

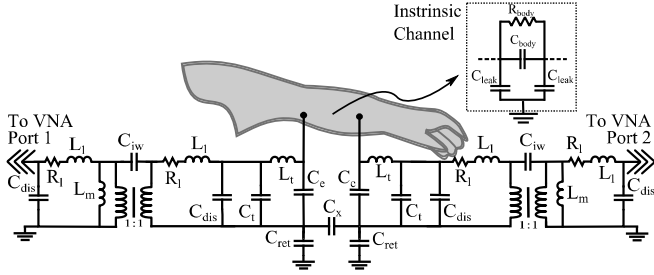


Fig. 14. Extended HBC channel model including primary channel, and fixtures model represented by the baluns T model and cable transition LC model.

The analysis of the circuit representing the extended model shows that the coupling capacitance C_{ret} , in the extrinsic part of the primary channel, and the interwinding capacitance C_{iw} , in the fixture part of the model, dominate the low frequency response, highly attenuating the signal. With the influence of C_{iw} , the cross capacitance of the electrode C_x becomes negligible, even for short distances. As the frequency increases, the impedance associated with these components drops considerably, approaching the impedance of the intrinsic part of the channel and increasing the gain. Thus, their combined effect now has to be taken into account. This can be attested by the fact that the distance of propagation over the body starts to affect the signal gain only at around 2-3 MHz. At this point the channel would become a high-pass filter if other components were neglected in the extended model. However, the combined effect of the parallel capacitances C_e , C_t and C_{dis} , from the electrodes, coaxial-to-PCB transition and baluns, respectively, and the series inductances L_l and L_t , from the baluns and coaxial-to-PCB transitions, control the cut-off frequency, giving the channel a band-pass profile. The leakage inductance series resistance, R_l , controls the band pass profile attenuation. The magnetizing inductance L_m should only influence the low frequency response, but its effect is masked by C_{iw} and C_{ret} . In accordance with the previous explanation, performing a systematic reduction procedure allows the identification of C_{dis} , L_l and C_{iw} as the dominant parameters up to 70 MHz, which can further result in a simplified valid version of the extended model. However, in this paper a full model is used for the sake of completeness.

If the test fixture model is completely omitted, the primary channel of Fig. 3 is restored and the correct primary channel response is found. The results show a considerably lower gain for the primary channel model, at least 43 dB lower than the gain for the extended model, in the whole low-pass frequency range, below 30 MHz. Also, only the intrinsic path continues to control the signal gain at high frequency, and the channel responds as a high-pass filter in the frequency range of interest. The channel gain for different propagation distances, $d = 20$ cm, 30 cm and 140cm, presents the followings trends: the gain of the signal is independent of the distance at low frequency (below 2-3 MHz) for the extended channel model, but not for the primary channel model. This happens due to C_x , which models the direct coupling between ground electrodes. Its low

value is not relevant when the fixtures add to the channel a large amount of capacitance through C_{iw} , but becomes critical when they are not present. At higher frequencies, for both models, the attenuation increases as the distance increases. In the next section these results will be compared with real channel measurements.

As can be seen, the inclusion of the test fixture should change the channel response considerably. The measurements discussed below support these results.

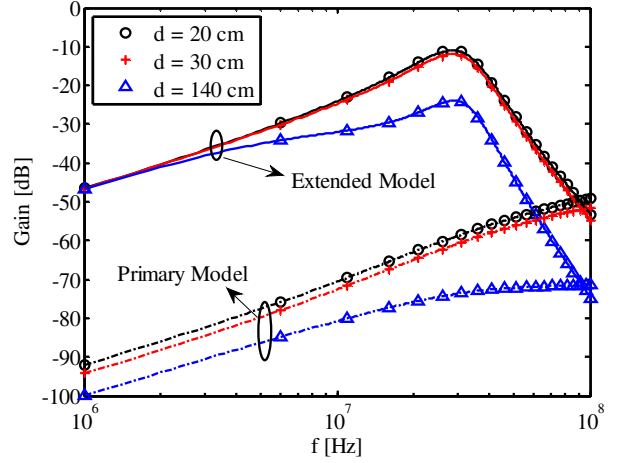


Fig. 15. HBC channel model response, comparing results from the primary channel model with those for the extended model, which includes the test fixture, for Balun A over frequency for propagation distances of $d = 20$ cm, 30 cm and 140 cm.

IV. EXPERIMENTAL VALIDATION OF THE MODEL

The measurements used in this section were taken with the setup described and modeled in Section III.A, and under the same conditions used to model the extrinsic channel part, i.e., the same ground electrode sizes, structures and distance from ground plane. The transmitter electrodes were placed on the wrist of one arm and the receiver electrodes positioned 15 cm and 30 cm away from it on the same arm, and 140 cm away on the wrist of the other arm, as in [24].

In Fig. 16, the results for the channel propagation over the distance are reported for two different baluns: Balun A (FTB-1-6) and Balun B (FTB-1-1). In general, the two sets of results show the same behavior, as explained in the previous section for the extended model. The channel gain profile resembles a band-pass filter, it is almost independent of distance below 5 MHz, with a peak gain of -10 dB at 28 MHz for Balun A and -14 dB at 42 MHz for Balun B, both for a 15 cm propagation distance. The important aspect to note here is the difference in gain according to the balun used. As mentioned previously, the balun interwinding capacitance C_{iw} boosts the signal gain [31]. Baluns with higher C_{iw} provide higher channel gain, as is the case for Balun A, with this difference being as large as 15 dB at below 25 MHz compared to Balun B. At this point it is important to note that some authors claim that the high frequency attenuation of the signal, which starts at around 30 MHz for the Balun A measurements and around 50 MHz for Balun B, is due

to attenuation of the surface wave portion of the signal coupled to the body [11], [16]. The extended model presented here does not include this effect, but shows a similar behavior for the frequency, as shown in Fig. 17 and Fig. 18. In fact, the model shows that this high frequency attenuation is probably connected to a resonance between the baluns, the electrodes and the coaxial-to-electrode transition inductances and capacitances. A comparison between the proposed models and measurements taken with Baluns A and B, for the propagation distance of 30 cm, is presented in Fig. 17 and Fig. 18.

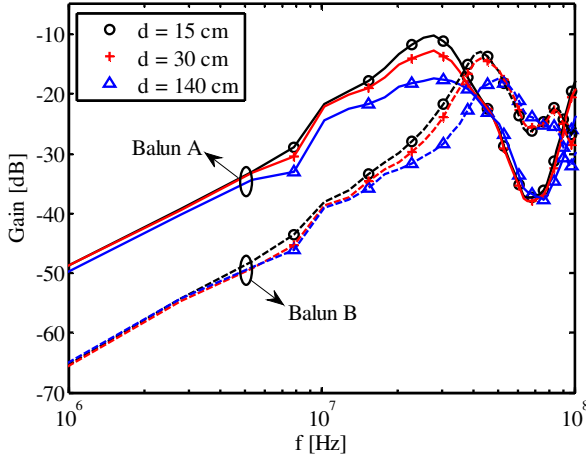


Fig. 16. Measurement results for different channel propagation distances: 15 cm (black), 30 cm (red) and 140 cm (blue) with Baluns A and B.

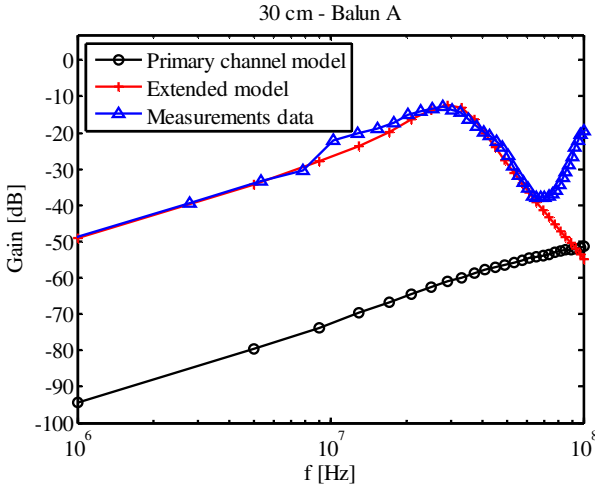


Fig. 17. Measurement and model simulation results for a channel propagation distance of 30 cm with Balun A.

Note that for Balun A, C_{iw} was reduced to 22 pF, which allows a better fitting between the data and the proposed model. In this way, the difference between the measurements and the extended model results in terms of the signal gain is always lower than 4 dB for frequencies of up to 70 MHz. This discrepancy could be attributed to the use of fixed values for the components of the model, which actually show some dependence on the frequency over the range investigated or to the variation

between the measurement subject biometric parameters and those used in the model [24]. For comparison purposes, the primary channel model simulation is presented on the same graph, clearly showing that the correct HBC channel response should be 45 dB lower in the worst case and should have a high-pass profile.

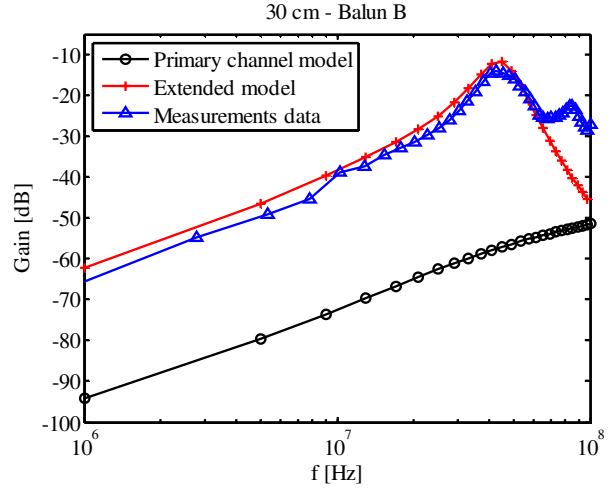


Fig. 18. Measurement and model simulation results for a channel propagation distance of 30 cm with Balun B.

For Balun B the results are similar. Overall, the extended model and measurement results show the same trends, with a good agreement for the frequency profile. The signal gain difference could be as high as 4 dB, at up to 70 MHz. Slightly reducing the balun parasitic capacitance C_{iw} to 7.5 pF, lowers the gain difference to less than 2.5 dB, in the same frequency range as before. Again, the difference between the measurements and the primary channel model results in terms of gain (as high as 43 dB) demonstrates the influence of the measurement setup, preventing the measurement of the correct channel response.

For both baluns the extended model proposed herein provides a good model-experiment correlation at up to 70 MHz. At above 70 MHz, the model almost always provides a lower value, while in the measurements the abrupt fall is interrupted by a new increase in the transmission, possibly arising from some non-modeled resonance or discontinuity [13].

To verify the model robustness regarding subject biometric characteristics variation, in Fig. 19, measurements of the channel frequency response are presented for two subjects against the prediction of the extended model. The subjects had about the same height, but different weight and body composition, the measurement setup included the Balun A and the electrodes were separated by 30 cm. Notice that the band pass profile and the peak frequency show a negligible difference for both subjects in channel attenuation up until 60 MHz. Also, the proposed model shows good agreement to the measured data, reasonably reproducing the frequency profile and attenuation levels up to 70 MHz.

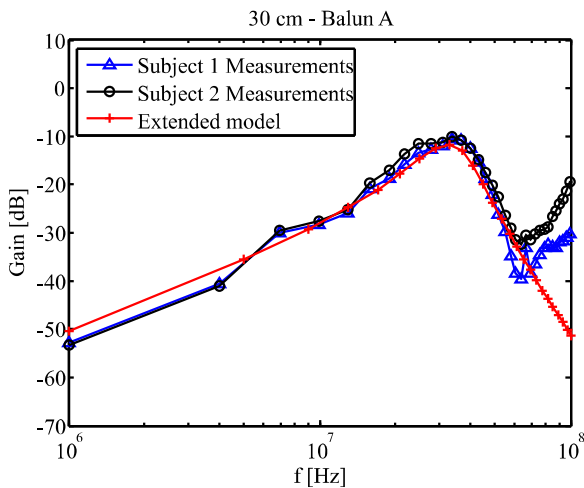


Fig. 19. Measurements for different subjects and extended model simulation results for a channel propagation distance of 30 cm with Balun A.

V. CONCLUSIONS

Research related to HBC spans almost two decades but there are several subjects related to channel characterization which still require elucidation. A central theme is the search for a general channel model which is effective for describing channel measurements and can aid the development of HBC transceivers. This study targeted the channel modeling problem by suggesting that the issues found in the models that represent the HBC channel through circuits, electromagnetic equations or other kinds of models, are not related to the primary channel model itself, but the fact that it does not consider some critical influences of the test fixture on the channel response. Initially, the division of the primary HBC channel into two parts (intrinsic and extrinsic) was proposed. This aided the identification and modeling of the essential channel components using distributed and lumped circuit representations which, despite being simple, provided a useful insight into the expected primary channel behavior. In general, the possibility of fixture calibration leads to some non-trivial effects being overlooked in channel characterization. It was verified in the literature and through tests that the effect of baluns, essential to preserving the channel return path when using grounded equipment, or the transition between coaxial cables and other parts of the setup, could not be easily accounted for through calibration alone. Thus, a measurement setup was assembled for channel characterization, and its parts were analyzed and modeled. The primary channel model was then extended to include the test fixture, and tested against channel measurements. This extended model achieved good results regarding the channel gain and frequency profiles, with differences of around 2-3 dB in channel gain for frequencies below 70 MHz, when compared to the measurements. Contrasting with these results, the intrinsic channel model shows that the expected gain was between 43-50 dB lower, showing the strong influence of the test fixture on the channel characterization. Since the modeling procedures adopted were based on the physical explanation of the components and phenomena present in the setup and primary channel, the developed model helps to properly describe the behavior of the channel measurements and provides a useful tool for gaining a

better understanding of the physical mechanisms associated with the channel response.

ACKNOWLEDGMENTS

The authors would like to thank to Kaléo Turnes Silvestri for assistance with the channel measurements and CNPq and INCT-NAMITEC for financial support.

REFERENCES

- [1] T. G. Zimmerman, "Personal Area Networks: Near-field intra-body communication", M.S. Thesis, MIT Media Laboratory, Cambridge, MA, Sept. 1995.
- [2] S. Yu. (2012, July 27). "IEEE introduces groundbreaking standard for body area networking" [Online]. Available: <http://standards.ieee.org/news/2012/ban.html>.
- [3] M.A Hanson, H.C. Powell, A. T. Barth, K. Ringgenberg, B. H. Calhoun, J. H. Aylor, J. Lach, "Body Area Sensor Networks: Challenges and Opportunities", *Computer*, vol.42, no.1, pp.58-65, Jan. 2009.
- [4] H. Baldus, S. Corroy, A. Fazzi, K. Klabunde, T. Schenk, "Human-centric connectivity enabled by body-coupled communications", *IEEE Commun. Mag.*, vol.47, no.6, pp.172-178, June 2009.
- [5] S.-H. Pun, Y.-M. Gao, P. U. Mak, M.-I. Vai, M. Du, "Quasi-Static Modeling of Human Limb for Intra-Body Communications With Experiments", *IEEE Trans. Inf. Technol. Biomed.*, vol.15, no.6, pp.870-876, Nov. 2011.
- [6] M. A Callejon, D. Naranjo-Hernandez, J. Reina-Tosina, L. M. Roa, "A Comprehensive Study Into Intrabody Communication Measurements", *IEEE Trans. Instrum. Meas.*, vol.62, no.9, pp.2446-2455, Sept. 2013.
- [7] M. S. Wegmueller, M. Oberle, N. Felber, N. Kuster, W. Fichtner, "Signal Transmission by Galvanic Coupling Through the Human Body", *IEEE Trans. Instrum. Meas.*, vol.59, no.4, pp.963-969, April 2010.
- [8] M.S. Wegmueller; S. Huclova, J. Froehlich, M. Oberle, N. Felber, N. Kuster, W. Fichtner, "Galvanic Coupling Enabling Wireless Implant Communications," *IEEE Trans. Instrum. Meas.*, vol.58, no.8, pp.2618-2625, Aug. 2009.
- [9] Y. Song; Q. Hao; K. Zhang; M. Wang; Y. Chu; B. Kang, "The Simulation Method of the Galvanic Coupling Intrabody Communication With Different Signal Transmission Paths," *IEEE Trans. Instrum. Meas.*, vol.60, no.4, pp.1257-1266, April 2011.
- [10] M. Amparo Callejon, D. Naranjo-Hernandez, J. Reina-Tosina, L. M. Roa, "Distributed Circuit Modeling of Galvanic and Capacitive Coupling for Intrabody Communication", *IEEE Trans. Biomed. Eng.*, vol.59, no.11, pp.3263-3269, Nov. 2012.
- [11] Z. Lucev, I. Krois, M. Cifrek, "A Capacitive Intrabody Communication Channel from 100 kHz to 100 MHz", *IEEE Trans. Instrum. Meas.*, vol.61, no.12, pp.3280-3289, Dec. 2012.
- [12] M. Seyedi, B. Kibret, D. T. H. Lai, M. Faulkner, "A Survey on Intrabody Communications for Body Area Network Applications", *IEEE Trans. Biomed. Eng.*, vol.60, no.8, pp.2067-2079, Aug. 2013.
- [13] R. Xu; H. Zhu; J. Yuan, "Electric-Field Intrabody Communication Channel Modeling With Finite-Element Method," *IEEE Trans. Biomed. Eng.*, vol.58, no.3, pp.705-712, March 2011.
- [14] R. Xu; H. Zhu; J. Yuan, "Characterization and analysis of intra-body communication channel," in *IEEE Antennas and Propagation Society Int. Symp.*, 2009, vol., no., pp.1-5, June 2009.
- [15] T. C. W. Schenk, N. S. Mazloum, L. Tan, P. Rutten, "Experimental characterization of the body-coupled communications channel", in *IEEE Int. Symp. on Wireless Communication Systems*, vol., no., pp.234-239, 21-24 Oct. 2008.
- [16] J. Bae; H. Cho; K. Song; H. Lee; H.-J. Yoo, "The Signal Transmission Mechanism on the Surface of Human Body for Body Channel Communication", *IEEE Trans. Microw. Theory Tech.*, vol.60, no.3, pp.582-593, March 2012.
- [17] J. A. Ruiz, S. Shimamoto, "Experimental Evaluation of Body Channel Response and Digital Modulation Schemes for Intra-body

- Communications", in *IEEE Int. Conf. on Communications*, vol.1, no., pp.349-354, June 2006.
- [18] N. Cho; Yoo, J.; S.-J. Song; J. Lee; S. Jeon; H.-J. Yoo, "The Human Body Characteristics as a Signal Transmission Medium for Intrabody Communication", *IEEE Trans. Microw. Theory Tech.*, vol.55, no.5, pp.1080-1086, May 2007.
- [19] W. D. Van Marken Lichtenbelt, K. R. Westerterp, L. Wouters, and S. C. M. Luijendijk, "Validation of bioelectrical-impedance measurements as a method to estimate body water compartments", *The American J. of Clinical Nutrition*, vol.60, no.2, pp.159-166, 1994.
- [20] B. Kibret; M. Seyedi; D. T. H. Lai, M. Faulkner, "Investigation of Galvanic-Coupled Intrabody Communication Using the Human Body Circuit Model", *IEEE J. of Biomedical and Health Informatics*, vol.18, no.4, pp.1196-1206, July 2014.
- [21] Cole, K., and Cole, R.: 'Dispersion and absorption in dielectrics', *The J. of Chemical Physics*, vol.9, no.2 pp. 341- 351, 1941.
- [22] M. A. Callejon, L. M. Roa, J. Reina-Tosina, D. Naranjo-Hernandez, "Study of Attenuation and Dispersion Through the Skin in Intrabody Communications Systems", *IEEE Trans. Inf. Technol. Biomed.*, vol.16, no.1, pp.159-165, Jan. 2012.
- [23] S. Gabriel, R.W. Lau, and C. Gabriel, "The dielectric properties of biological tissues: III. Parametric models for the dielectric spectrum of tissues," *Physics in Medicine and Biology*, vol. 41, pp. 2271-2293, 1996.
- [24] M. D. Pereira, K. T. Silvestri, F. R. de Sousa, "Measurement results and analysis on a HBC channel", in *IEEE Int. Symp. on Medical Measurements and Applications (MeMeA)*, vol., no., pp.11-12, June 2014.
- [25] K. Hachisuka, T. Takeda, Y. Terauchi, K. Sasaki, H. Hosaka, K. Itao, "Intra-body data transmission for the personal area network", *Microsystem Technologies*, vol.11, no.(8-10), 1020-1027, 2005.
- [26] H.; Nakamura, M., "Form and capacitance of parallel-plate capacitors", *IEEE Trans. Compon. Packag. Manuf. Technol. A*, vol.17, no.3, pp.477-484, Sep 1994.
- [27] R. Xu; W. C. Ng; H. Zhu; H. Shan; J. Yuan, "Equation Environment Coupling and Interference on the Electric-Field Intrabody Communication Channel", *IEEE Trans. Biomed. Eng.*, vol.59, no.7, pp.2051-2059, July 2012.
- [28] Y. M. Chi, T.-P. Jung; G. Cauwenberghs, "Dry-Contact and Noncontact Biopotential Electrodes: Methodological Review", *IEEE Reviews in Biomedical Engineering*, vol.3, no., pp.106-119, 2010.
- [29] G. S. Anderson, C. G. Sodini, "Body coupled communication: The channel and implantable sensors," in *IEEE Int. Conf. on Body Sensor Networks*, vol., no., pp.6-9, May 2013.
- [30] *De-embedding and Embedding S-Parameter Networks Using a Vector Network Analyzer*, Appl. Note 1364-1, Agilent Technologies, 2004.
- [31] J. Sakai, L.-S. Wu; H.-C. Sun; Y.-X. Guo, "Balun's effect on the measurement of transmission characteristics for intrabody communication channel," in *IEEE Int. Microwave Workshop Series on RF and Wireless Technologies for Biomedical and Healthcare Applications (IMWS-BIO)*, vol., no., pp. 9-11 Dec. 2013.
- [32] L. Sun; Y. Chen; K. Sun; W. Wu, "Analysis of differential balun circuits", in *Int. Symp. on Signals Systems and Electronics (ISSSE)*, vol.1, no., pp.17-20 Sept. 2010.
- [33] Colonel Wm. T. McLyman, *Transformer And Inductor Design Handbook*, 3rd ed., Idyllwild, California: Kg Magnetics, Inc., 2004.
- [34] *Impedance Measurement Handbook: A Guide to Measurement Technology and Techniques*, 4th ed., Agilent Technologies, December 2003.